sustainability

Article

New Insight into the Depositional Age of No. 6 Coal in Heidaigou Mine, Late Paleozoic Jungar Coalfield, Inner Mongolia, China

Chao Liu [1,2], Xiangdong Chang [1,2], Beilei Sun [1,2,*] and Fangui Zeng [1,2]

[1] College of Mining Engineering, Taiyuan University of Technology, Taiyuan 030024, China; liuchao06@tyut.edu.cn (C.L.); changxiangdong0586@link.tyut.edu.cn (X.C.); zengfangui@tyut.edu.cn (F.Z.)
[2] Shanxi Key Laboratory of Coal and Coal Measure Gas Geology, Taiyuan 030024, China
* Correspondence: sunbeilei@tyut.edu.cn

Abstract: Coal deposits can provide novel stratigraphic markers for reconstructing the evolution history of a sedimentary basin and correlating sedimentary successions. Age dating was conducted on zircons harvested from the No. 6 coal seam within the Heidaigou Mine, Inner Mongolia. Two-kilogram samples were taken, and the recovered zircons were analyzed for U–Pb isotopic and rare earth elements (REE). The REE results of the zircon grains showed that all the zircon grains were enriched in heavy rare earth elements (HREE) but depleted in light rare earth elements (LREE). In addition, zircons from the No. 6 coal seam had strongly positive Ce (Ce/Ce* = 2.4–224.6) and strongly negative Eu anomalies (Eu/Eu* = 0.1–0.6). Combined with the clear oscillatory zones in the cathodoluminescence images, all the zircon grains of the No. 6 coal were characteristic of zircons with magmatic origins. The $^{206}Pb/^{238}U$ ages of 34 zircon grains produced a narrow age population of 303–286 Ma, with a weighted average age of 293.0 $\pm$ 1.5 Ma (mean-squared weighted deviation = 1.5). Therefore, we infer that the No. 6 coal in the Heidaigou Mine was deposited during the Early Permian, and the Carboniferous–Permian boundary should be located stratigraphically lower than the No. 6 coal. The zircon U–Pb geochronology is a useful tool to determine the depositional ages of non-marine-influenced coal.

Keywords: Heidaigou Mine; No. 6 coal; depositional age; zircon U–Pb dating; rare earth element

check for updates

Citation: Liu, C.; Chang, X.; Sun, B.; Zeng, F. New Insight into the Depositional Age of No. 6 Coal in Heidaigou Mine, Late Paleozoic Jungar Coalfield, Inner Mongolia, China. *Sustainability* **2022**, *14*, 6297. https://doi.org/10.3390/su14106297

Academic Editor: Marco Lezzerini

Received: 12 April 2022
Accepted: 19 May 2022
Published: 21 May 2022

1. Introduction

Coal is an organic sedimentary rock; determining its accurate depositional age will help us to reconstruct the evolution history of the sedimentary deposits [1]. In general, the magnetic stratigraphic method [2], oil generation capacity of coals [3,4], palynology of coal [5], radiometric dating of tonstein [6], and Re–Os isotopic analysis [1,7] can be used to determine coal depositional age. Recently, Tripathy et al. [1] proposed that the Re–Os isotopic analysis was a viable method of dating organic-rich sediments; whereas for terrestrial coals, the Re–Os age was not useful for determining the depositional ages because of the highly heterogeneous nature of the initial Os isotopic composition [7]. It is a challenge to obtain the direct age of non-marine-influenced coals in which there is no tonstein. With the improvement in analytical techniques and the development of Multi-Collector Laser Ablation Inductively Coupled Plasma Mass Spectrometry (MC-LA-ICP-MS), U–Pb isotopic analyses of single detrital zircon grains in sedimentary strata have become popular for determining the maximum depositional ages of host sediments [8–11], especially for the strata-absent preserved fossils [12] and biostratigraphic age controlling [13].

The Heidaigou Mine is one of the largest coal mines in the Jungar Coalfield, northeast of the Ordos basin, in North China (Figure 1). No. 6 coal, the main mineable coal seam, is well-known because of its high gallium (Ga) contents, which have reached industrial grade [14,15]. The gallium in No. 6 coal mainly occurred in clay minerals, such as boehmite and kaolinite [14]. It is generally considered that the concentration of Ga is associated with bauxite from the Benxi Formation and Middle Proterozoic moyite of the Yinshan Oldland [14,15] and that it also would be controlled by the depositional environment, organic material, tectonic activities, and some other factors [16]. The exact depositional age of No. 6 coal is helpful to understand the depositional process and the source materials of No. 6 coal. Wang [17] found Lycospora pusilla, Reinschospora triangulata, Ahrensisporite querickei, Torispora securis, Striatosporites major, etc., in the Taiyuan Formation, Jungar coalfield, and these sporopollen assemblages belong to the late Carboniferous. However, Yang et al. [18] suggested No. 6 coal was formed during the early Permian, owing to the discovery of early Permian T. multinervis. Jia [19] analyzed the sporopollens in the No. 6 coal, gangue, roof, and floor rocks and presented an assemblage of Gulisporites–Thymosporites–Cyclogranisporites–Laevigatosporites–Florinites with a transition from the late Carboniferous to early Permian. In this context, the MC-LA-ICP-MS was used to test the U–Pb isotopic composition and rare earth element characteristics of detrital zircon grains from the No. 6 coal of the Heidaigou mine to accurately ascertain the depositional age of the No. 6 coal.

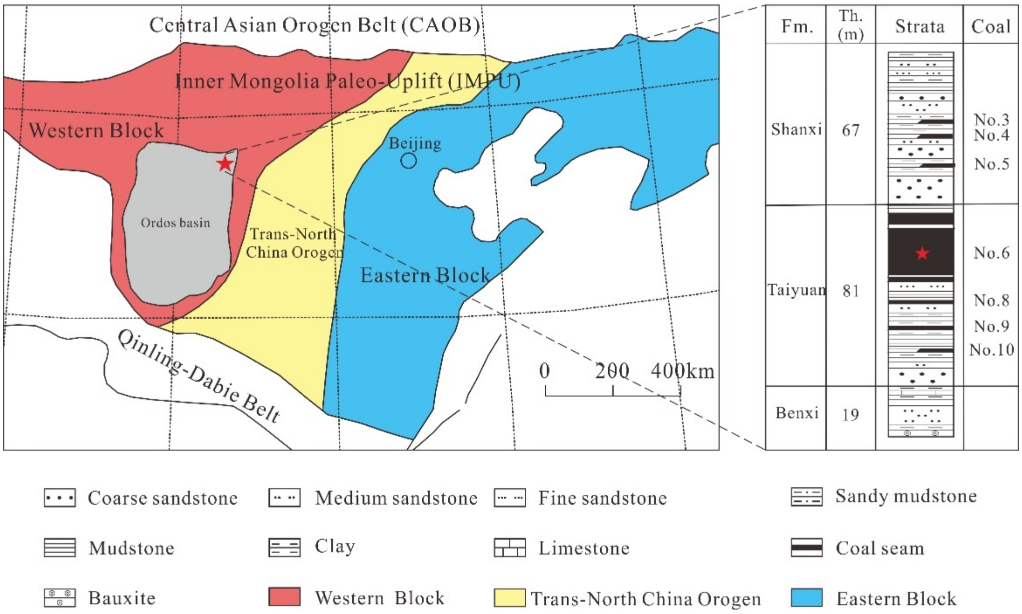

Figure 1. Geological sketch map of the North China Craton (modified after Zhao et al., 2005) [20] and sampling locations (Fm.: Formation, Th.: Thickness).

2. Geological Setting and Sample Description

The Ordos Basin is located in the western part of the North China Craton. The basin is an intracontinental depression in the North China Craton from the late Paleozoic, and the coal-bearing strata are developed extensively. The Heidaigou Mine is located in the eastern margin of the Jungar Coalfield. The Late Paleozoic coal-bearing deposits of the basin consist of the Benxi, Taiyuan, and Shanxi Formations (Figure 1) with thicknesses of 19 m, 81 m, and 67 m, respectively (Figure 1b). The Benxi Formation, non-conformably overlying the Middle Ordovician Majiagou limestone [14], is mainly composed of gray bauxite, limestone, and sandstone. The Taiyuan Formation is mainly composed of grayish-white medium-grained quartzose sandstone, limestone, siltstone, coal, and mudstone. No. 6 coal is located at the uppermost Taiyuan Formation, with a thickness of 20 m. The roof of the No. 6 coal mine is mudstone, sandy mudstone, or siltstone, and the floor is mudstone. The Shanxi Formation is composed of gray sandstone, mudstone, siltstone, and five coal seams (Nos. 1, 2, 3, 4, and 5), but these coal seams are not minable [15]. In this study, one coal-seam sample was collected from the No. 6 coal seam in the Heidaigou Mine, following the Chinese Standard Method GB482-2008 [20]. The coal sample was a high volatile (~33.5%) and low–medium ash yield (~17.5%) bituminous coal with a vitrinite reflectance value of 0.58% [14]. The minerals in the coal were mainly kaolinite, boehmite, and minor calcite (Figure 2).

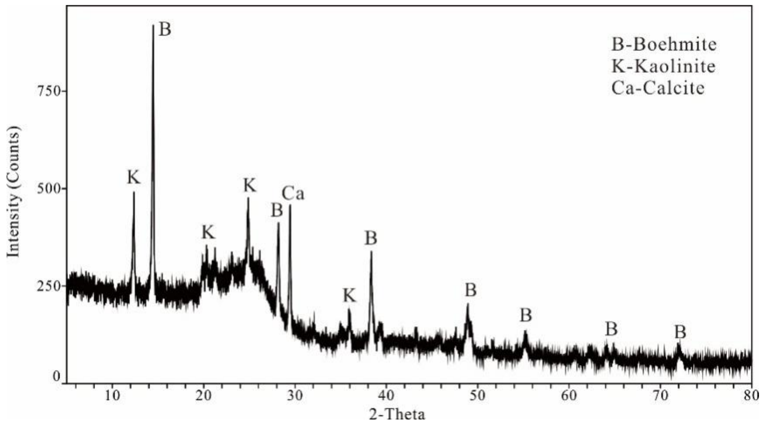

Figure 2. X-ray powder diffraction pattern of No. 6 coal, Heidaigou coal mine, performed by Ultima IV power 172 diffractometer (Rigaku, Tokyo, Japan).

3. Analysis Methods

X-ray powder diffraction (XRD) analysis was performed on an Ultima IV power diffractometer (Rigaku, Tokyo, Japan) with Ni-filtered Cu–K radiation and a scintillation detector. Each XRD pattern was recorded over a 2θ interval of 5–90° with a step size of 0.02°. X-ray diffractograms were subjected to quantitative mineralogical analysis using the PDXLTM interpretation software system (Rigaku, Tokyo, Japan).

Two-kilogram coal samples were crushed, pulverized, and sieved using meshes of 0.074 mm. The pulverized sample was used to concentrate the heavy minerals by a Wilfley table, which were then further separated magnetically and with a heavy liquid. Zircon grains were separated under a binocular microscope, mounted in epoxy resin, and polished down to expose the grain centers. All zircon grains were inspected by cathodoluminescence (CL) imaging to characterize their internal textures. Zircons with inherited cores were excluded during the U–Pb analyzing. U–Pb dating and trace element analyses were performed on an Analytik Jena Plasma Quant MS Elite ICP-MS (MC-LA-ICP-MS), coupled with a New Wave Research 193 nm laser microprobe at the Beijing Createch Testing Technology Co., Ltd. For trace element content calibration, the NIST SRM 610 was analyzed as the external standard, and Si was analyzed as the internal standard. The raw data reduction and age calculation were analyzed using the program ICPMSDataCal [21]. The interpretation of the zircon age was based on the $^{206}Pb/^{208}U$ ages for grains <1000 Ma and on $^{206}Pb/^{207}Pb$ for grains >1000 Ma. Isoplot 4.0 software was used to undertake the age calculation and Concordia diagrams [22].

4. Zircon Geochronology and Geochemistry

The zircon crystals within 50 to 150 µm in size were subhedral to euhedral (Figure 3). All zircon grains displayed clear oscillatory zones in the CL images and had high Th/U ratios (0.56–1.55, Figure 4, Table 1), indicating that they were magmatic zircons. A total of 34 out of 40 analyzed spots acquired the $^{206}Pb/^{238}U$ concordant ages in a narrow age population of 303–286 Ma, defining a single peak age with a weighted average age of 293.0 ± 1.5 Ma (MSWD = 1.5, Figure 5).

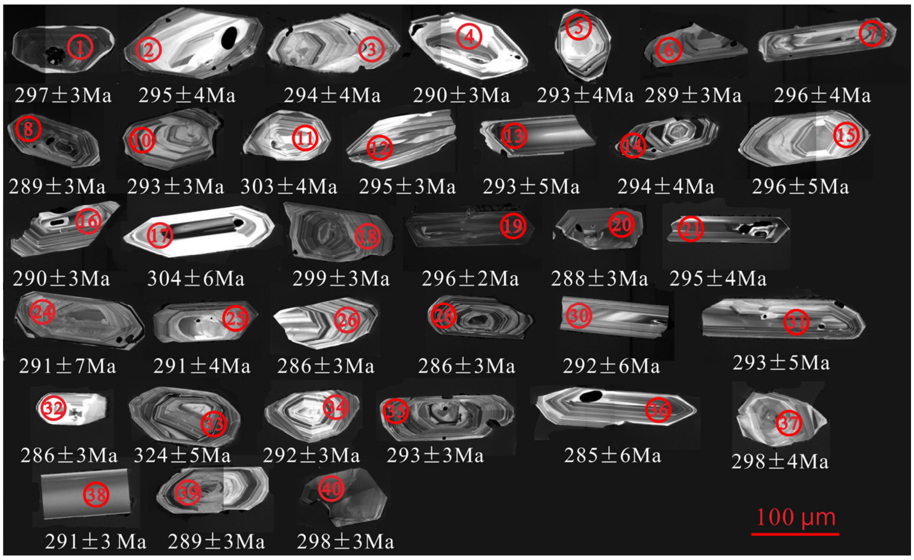

Figure 3. All cathodoluminescence images of zircons from the No. 6 coal sample, showing the analysis spots in the red circles.

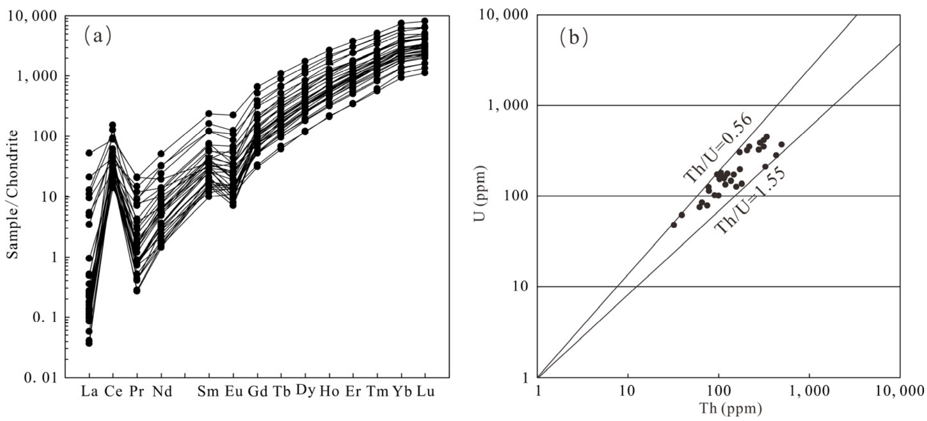

Figure 4. Chondrite normalized REE patterns (**a**) and Th/U ratios (**b**) of zircon grains in No. 6 coal, Heidaigou coal mine.

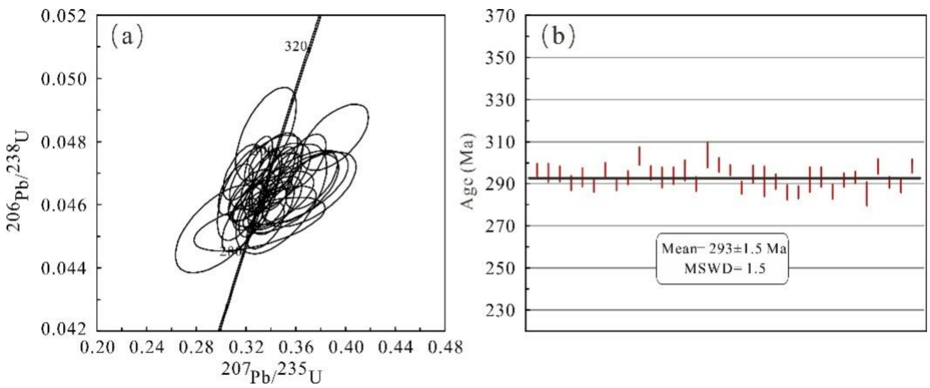

Figure 5. U–Pb concordia diagram (**a**) and weighted-average age diagram (**b**) of single-grain zircon LA-ICP-MS analysis for the No. 6 coal, Heidaigou coal mine, performed by an Analytik Jena Plasma Quant MS Elite ICP-MS.

Table 1. Results of the LA-ICP-MS U-Pb isotopic analysis for detrital zircons in No. 6 coal, Heidaigou Mine.

Spots	Th (232)	U (238)	$^{207}Pb/^{206}Pb$		$^{207}Pb/^{235}U$		$^{206}Pb/^{238}U$		$^{208}Pb/^{232}Th$		$^{207}Pb/^{206}Pb$		$^{207}Pb/^{235}U$		$^{206}Pb/^{238}U$		$^{208}Pb/^{232}Th$		*Concor.*
	ppm	*ppm*	*Ratio*	$\pm\sigma$	*Ratio*	$\pm\sigma$	*Ratio*	$\pm\sigma$	*Ratio*	$\pm\sigma$	*Age (Ma)* $\pm\sigma$		*Age (Ma)* $\pm\sigma$		*Age (Ma)* $\pm\sigma$		*Ratio*	$\pm\sigma$	
DHG-1-01	353.8	44.4	0.0536	0.0011	0.3480	0.0076	0.0471	0.0005	0.0138	0.0004	353.8	44.4	303.2	5.7	296.7	3.0	276.9	7.9	97%
DHG-1-02	350.1	122.2	0.0535	0.0028	0.3437	0.0183	0.0469	0.0007	0.0132	0.0004	350.1	122.2	300.0	13.9	295.3	4.4	264.8	8.5	98%
DHG-1-03	524.1	71.3	0.0579	0.0020	0.3726	0.0137	0.0468	0.0006	0.0133	0.0004	524.1	71.3	321.6	10.2	294.7	3.7	267.8	8.7	91%
DHG-1-04	368.6	90.7	0.0539	0.0022	0.3432	0.0142	0.0461	0.0006	0.0141	0.0004	368.6	90.7	299.6	10.7	290.3	3.4	283.1	8.0	96%
DHG-1-05	501.9	132.4	0.0573	0.0033	0.3637	0.0203	0.0465	0.0007	0.0140	0.0006	501.9	132.4	314.9	15.1	293.1	4.4	280.7	12.5	92%
DHG-1-06	405.6	118.5	0.0548	0.0029	0.3470	0.0194	0.0458	0.0005	0.0143	0.0006	405.6	118.5	302.5	14.6	289.0	3.0	287.0	11.1	95%
DHG-1-07	150.1	70.4	0.0490	0.0015	0.3171	0.0102	0.0470	0.0006	0.0141	0.0004	150.1	70.4	279.7	7.9	296.3	3.6	282.3	8.4	94%
DHG-1-08	366.7	55.6	0.0537	0.0013	0.3397	0.0086	0.0459	0.0004	0.0133	0.0004	366.7	55.6	297.0	6.5	289.4	2.6	266.5	7.9	97%
DHG-1-09	153.8	477.7	0.0491	0.0116	0.3159	0.0742	0.0470	0.0012	0.0148	0.0033	153.8	477.7	278.7	57.3	296.3	7.6	296.1	65.4	93%
DHG-1-10	131.6	68.5	0.0487	0.0014	0.3115	0.0092	0.0465	0.0005	0.0137	0.0005	131.6	68.5	275.3	7.1	292.9	3.3	275.3	9.7	93%
DHG-1-12	388.9	50.0	0.0542	0.0012	0.3505	0.0094	0.0468	0.0005	0.0141	0.0004	388.9	50.0	305.1	7.0	295.1	3.2	282.9	7.6	96%
DHG-1-13	524.1	131.5	0.0578	0.0035	0.3707	0.0249	0.0465	0.0008	0.0155	0.0007	524.1	131.5	320.2	18.5	292.9	4.8	311.3	14.7	91%
DHG-1-14	300.1	51.8	0.0522	0.0012	0.3349	0.0081	0.0466	0.0006	0.0145	0.0004	300.1	51.8	293.3	6.1	293.8	3.9	290.9	8.0	99%
DHG-1-15	287.1	131.5	0.0520	0.0030	0.3364	0.0194	0.0470	0.0008	0.0155	0.0007	287.1	131.5	294.4	14.7	296.2	4.8	311.0	13.4	99%
DHG-1-16	276.0	86.1	0.0518	0.0019	0.3267	0.0115	0.0460	0.0005	0.0143	0.0004	276.0	86.1	287.0	8.8	289.9	3.2	287.4	7.5	99%
DHG-1-17	235.3	114.8	0.0509	0.0025	0.3362	0.0161	0.0482	0.0010	0.0151	0.0005	235.3	114.8	294.3	12.2	303.7	6.0	302.0	9.4	96%
DHG-1-18	298.2	81.5	0.0523	0.0019	0.3420	0.0130	0.0475	0.0005	0.0144	0.0004	298.2	81.5	298.7	9.9	298.9	3.3	289.2	7.8	99%
DHG-1-19	353.8	56.5	0.0536	0.0015	0.3474	0.0097	0.0470	0.0004	0.0147	0.0004	353.8	56.5	302.7	7.3	296.4	2.4	295.5	7.9	97%
DHG-1-20	279.7	55.6	0.0519	0.0013	0.3268	0.0083	0.0457	0.0005	0.0139	0.0004	279.7	55.6	287.2	6.3	288.2	3.0	279.9	8.6	99%
DHG-1-21	298.2	50.0	0.0523	0.0011	0.3366	0.0079	0.0467	0.0007	0.0149	0.0004	298.2	50.0	294.6	6.0	294.5	4.2	299.2	7.8	99%
DHG-1-24	413.0	177.8	0.0551	0.0043	0.3484	0.0242	0.0462	0.0011	0.0120	0.0008	413.0	177.8	303.5	18.2	291.1	7.1	242.1	15.5	95%
DHG-1-25	366.7	144.4	0.0537	0.0035	0.3417	0.0217	0.0462	0.0006	0.0164	0.0006	366.7	144.4	298.4	16.4	291.0	3.6	328.3	12.5	97%
DHG-1-26	220.4	66.7	0.0505	0.0015	0.3155	0.0097	0.0454	0.0006	0.0147	0.0004	220.4	66.7	278.4	7.5	285.9	3.5	295.6	8.6	97%
DHG-1-28	364.9	67.6	0.0539	0.0017	0.3356	0.0100	0.0453	0.0005	0.0147	0.0005	364.9	67.6	293.9	7.6	285.9	3.0	294.2	9.6	97%
DHG-1-30	198.2	98.1	0.0501	0.0021	0.3182	0.0142	0.0463	0.0010	0.0156	0.0007	198.2	98.1	280.5	10.9	292.0	6.0	312.0	13.2	95%
DHG-1-31	453.8	149.1	0.0560	0.0039	0.3605	0.0275	0.0465	0.0008	0.0166	0.0010	453.8	149.1	312.6	20.5	293.3	4.8	332.8	19.9	93%
DHG-1-32	320.4	237.0	0.0528	0.0055	0.3308	0.0349	0.0454	0.0006	0.0148	0.0009	320.4	237.0	290.2	26.6	286.1	3.5	297.3	17.2	98%
DHG-1-34	242.7	88.9	0.0510	0.0019	0.3246	0.0123	0.0463	0.0005	0.0150	0.0005	242.7	88.9	285.4	9.5	291.8	3.3	301.1	9.1	97%
DHG-1-35	366.7	57.4	0.0537	0.0014	0.3437	0.0091	0.0465	0.0005	0.0152	0.0004	366.7	57.4	300.0	6.9	293.0	2.9	305.3	8.9	97%

Table 1. *Cont.*

Spots	Th (232)	U (238)	^{207}Pb/^{206}Pb		^{207}Pb/^{235}U		^{206}Pb/^{238}U		^{208}Pb/^{232}Th		^{207}Pb/^{206}Pb		^{207}Pb/^{235}U		^{206}Pb/^{238}U		^{208}Pb/^{232}Th		*Concor.*
DHG-1-36	87.1	166.6	0.0478	0.0035	0.2991	0.0237	0.0452	0.0009	0.0152	0.0005	87.1	166.6	265.7	18.5	285.2	5.7	305.7	9.8	92%
DHG-1-37	453.8	66.7	0.0561	0.0016	0.3664	0.0118	0.0474	0.0006	0.0152	0.0004	453.8	66.7	317.0	8.8	298.3	3.6	304.6	8.9	93%
DHG-1-38	213.0	66.7	0.0504	0.0014	0.3204	0.0095	0.0461	0.0004	0.0156	0.0004	213.0	66.7	282.2	7.3	290.7	2.7	313.3	8.7	97%
DHG-1-39	372.3	66.7	0.0540	0.0016	0.3420	0.0110	0.0459	0.0006	0.0158	0.0005	372.3	66.7	298.7	8.3	289.3	3.4	316.9	10.8	96%
DHG-1-40	233.4	51.8	0.0507	0.0012	0.3301	0.0074	0.0474	0.0005	0.0162	0.0005	233.4	51.8	289.7	5.7	298.4	3.2	324.4	10.0	97%

The chondrite-normalized REE pattern (Figure 5) revealed distinctively heavy rare earth elements (HREE) enriched in comparison with the light rare earth elements (LREE) characterized by LREE/HREE within 0.02–0.10 (Table 2). It also showed strongly positive Ce anomalies (Ce/Ce* = 2.4–224.6) and negative Eu anomalies (Eu/Eu* = 0.1–0.6). These data support that the zircon grains of the No. 6 coal had the common characteristics of magmatic zircons [23,24]. When plotting the REE data of these zircon grains on Y vs. U/Yb and Hf vs. U/Yb diagrams, all zircons fell in the continental zircon field (Figure 6a,b). In addition, the Y vs. U, Nb/Ta vs. Yb/Sm, and Nb vs. Ta diagrams indicated the majority had characteristics of zircons in intermediate-acid igneous rocks, such as granitoids and syenite pegmatites (Figure 6c–f).

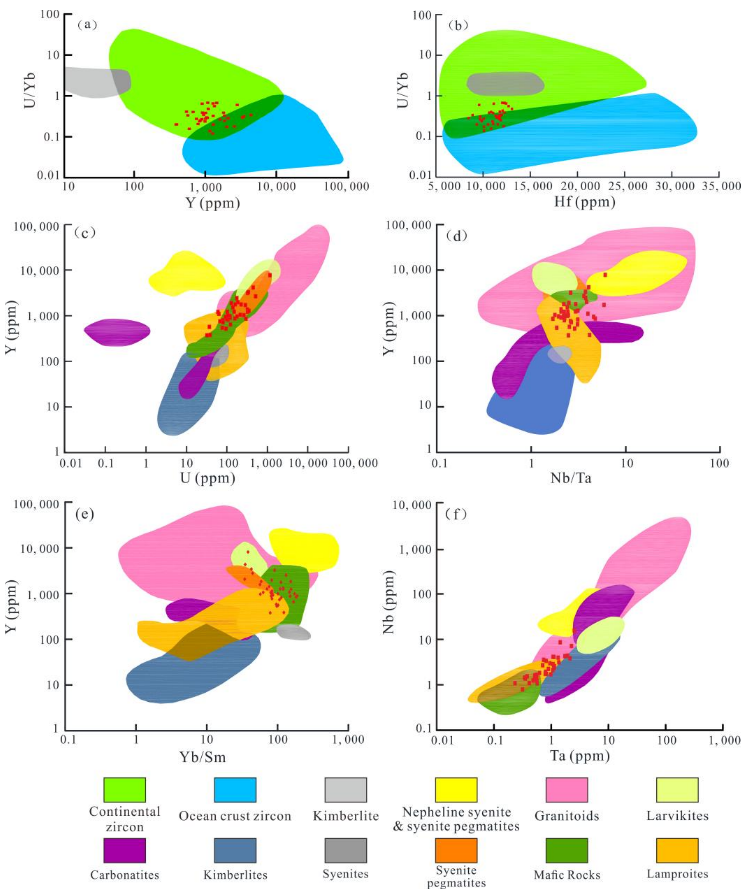

Figure 6. Binary diagrams of trace element concentrations and ratios for the zircon grains from No. 6 coal, Heidaigou coal mine (following Belousova et al., 2002) [24]. (**a**) The diagram of Y vs. U–Yb, (**b**) the diagram of Hf vs. U/Yb, (**c**) the diagram of U vs. Y, (**d**) the diagram of Nb/Ta vs. Y, (**e**) the diagram of Yb/Sm vs. Y, (**f**) the diagram of Ta vs. Nb.

Table 2. Results of rare earth elements for detrital zircons in No. 6 coal, Heidaigou Mine.

Sample No.	La	Ce	Pr	Nd	Sm	Eu	Gd	Tb	Dy	Ho	Er	Tm	Yb	Lu	Hf	Ta	Hg	Nb	Y
	ppm	ppm	ppm	ppm	ppm	ppm	ppm	ppm	ppm	ppm	ppm	ppm	ppm	ppm	ppm	ppm	ppm	ppm	ppm
DHG-1-01	0.01	14.08	0.17	2.94	6.09	1.11	29.73	10.65	129.36	48.27	212.87	47.91	465.55	2.38	0.01	14.08	0.17	2.38	1396.7
DHG-1-02	0.03	15.92	0.08	1.03	2.21	0.83	10.82	3.54	45.47	17.63	82.79	20.94	226.33	1.07	0.03	15.92	0.08	1.07	547.9
DHG-1-03	0.08	9.80	0.07	1.46	2.87	0.74	13.85	5.35	66.93	26.39	124.25	30.79	325.26	1.81	0.08	9.80	0.07	1.81	801.5
DHG-1-04	0.04	15.80	0.13	2.97	4.63	2.04	22.53	8.28	104.15	41.16	193.23	47.05	506.24	1.65	0.04	15.80	0.13	1.65	1248.3
DHG-1-05	0.02	13.56	0.04	0.80	2.01	0.77	6.89	2.53	29.86	12.35	56.42	14.37	158.93	0.79	0.02	13.56	0.04	0.79	374.3
DHG-1-06	0.12	18.70	0.15	3.56	6.38	1.15	24.92	9.00	110.22	41.57	185.43	44.32	455.76	2.31	0.12	18.70	0.15	2.31	1243.7
DHG-1-07	0.03	12.94	0.03	0.67	2.22	0.40	14.97	6.17	83.30	33.81	156.29	36.93	387.67	2.09	0.03	12.94	0.03	2.09	975.1
DHG-1-08	1.13	33.28	0.37	3.06	4.01	0.68	23.28	8.20	104.08	40.93	193.02	45.95	484.79	4.26	1.13	33.28	0.37	4.26	1238.9
DHG-1-09	0.00	13.80	0.07	0.72	1.52	0.64	6.35	2.31	30.44	11.84	57.58	15.33	188.15	1.43	0.00	13.80	0.07	1.43	381.3
DHG-1-10	0.03	31.81	0.05	0.88	2.24	0.92	11.22	4.36	60.83	25.93	134.69	35.46	411.90	2.96	0.03	31.81	0.05	2.96	828.2
DHG-1-12	0.81	37.34	0.86	10.99	18.53	4.95	79.96	25.11	278.79	96.87	399.15	86.18	829.20	4.06	0.81	37.34	0.86	4.06	2717.8
DHG-1-13	0.01	13.96	0.22	3.67	8.64	3.10	39.27	14.41	174.85	66.02	296.02	68.23	718.83	1.36	0.01	13.96	0.22	1.36	1926.4
DHG-1-14	3.05	78.71	0.73	4.73	5.03	1.48	21.17	7.79	100.83	41.34	209.10	54.65	608.02	7.08	3.05	78.71	0.73	7.08	1297.1
DHG-1-15	0.07	19.27	0.13	2.37	3.82	1.48	15.56	5.09	62.37	24.70	118.86	29.31	320.91	1.08	0.07	19.27	0.13	1.08	762.1
DHG-1-16	0.03	14.88	0.30	5.22	9.15	2.52	38.81	13.22	151.74	54.40	234.10	52.64	519.18	1.34	0.03	14.88	0.30	1.34	1550.8
DHG-1-17	0.03	8.45	0.18	2.78	5.35	1.32	21.54	7.73	95.11	36.25	169.18	40.80	449.51	1.52	0.03	8.45	0.18	1.52	1115.2
DHG-1-18	0.01	12.11	0.03	0.75	2.37	0.46	13.24	5.46	72.25	30.17	143.76	34.21	358.25	1.68	0.01	12.11	0.03	1.68	864.5
DHG-1-19	1.29	16.01	0.66	6.43	11.58	1.99	67.93	24.83	309.26	117.46	509.32	111.26	1059.37	2.83	1.29	16.01	0.66	2.83	3218.3
DHG-1-20	0.00	11.44	0.08	1.59	4.32	0.56	28.08	11.50	155.04	64.29	292.79	66.20	665.16	3.93	0.00	11.44	0.08	3.93	1794.8
DHG-1-21	2.62	56.93	1.90	23.89	36.39	12.92	136.98	40.82	445.05	150.57	621.17	133.38	1280.63	3.33	2.62	56.93	1.90	3.33	4237.8
DHG-1-24	0.05	11.26	0.07	1.61	3.94	1.07	17.45	6.59	81.68	32.70	150.09	33.88	341.78	1.73	0.05	11.26	0.07	1.73	913.7
DHG-1-25	0.22	11.51	0.07	1.47	2.69	0.88	14.21	4.82	64.84	24.22	113.83	26.96	287.28	1.37	0.22	11.51	0.07	1.37	725.1
DHG-1-26	0.04	93.30	0.11	2.28	6.40	3.56	31.72	11.24	143.59	56.47	272.23	66.11	718.67	8.51	0.04	93.30	0.11	8.51	1743.5
DHG-1-28	12.46	54.13	1.97	8.87	5.47	1.77	15.95	5.26	63.80	26.31	134.64	37.71	446.15	3.52	12.46	54.13	1.97	3.52	870.4
DHG-1-30	2.24	23.92	1.40	15.06	18.35	6.40	64.90	19.52	209.45	72.19	292.34	64.91	634.99	1.37	2.24	23.92	1.40	1.37	2018.1
DHG-1-31	4.91	27.29	1.12	6.49	4.65	0.81	20.69	7.13	88.67	33.58	151.52	36.63	388.74	1.92	4.91	27.29	1.12	1.92	1001.6
DHG-1-32	0.00	21.08	0.28	4.06	6.68	2.02	24.05	7.21	82.77	30.50	143.47	35.23	383.59	1.07	0.00	21.08	0.28	1.07	956.2
DHG-1-33	0.08	26.52	0.10	1.03	2.31	0.65	9.22	3.44	41.09	16.81	80.30	21.14	226.83	1.81	0.08	26.52	0.10	1.81	524.0
DHG-1-34	0.05	26.85	0.08	1.33	1.75	0.80	10.97	3.98	49.67	20.40	101.42	26.37	296.59	1.61	0.05	26.85	0.08	1.61	648.8
DHG-1-35	0.03	25.21	0.04	1.34	2.92	0.45	16.09	6.91	87.85	34.71	166.68	41.75	431.14	4.34	0.03	25.21	0.04	4.34	1061.3

Table 2. *Cont.*

Sample No.	La	Ce	Pr	Nd	Sm	Eu	Gd	Tb	Dy	Ho	Er	Tm	Yb	Lu	Hf	Ta	Hg	Nb	Y
	ppm	ppm	ppm	ppm	ppm	ppm	ppm	ppm	ppm	ppm	ppm	ppm	ppm	ppm	ppm	ppm	ppm	ppm	ppm
DHG-1-36	0.02	17.45	0.40	5.96	10.85	3.92	46.88	15.04	173.46	62.87	276.00	65.37	640.96	1.25	0.02	17.45	0.40	1.25	1804.0
DHG-1-37	0.02	13.06	0.08	1.69	4.39	0.57	22.19	7.96	96.02	35.67	159.77	36.00	353.38	2.21	0.02	13.06	0.08	2.21	1033.3
DHG-1-38	0.11	30.43	0.85	14.63	24.57	7.23	106.43	32.76	359.39	124.89	510.81	110.62	1055.61	2.68	0.11	30.43	0.85	2.68	3372.2
DHG-1-39	0.06	20.88	0.16	2.57	4.44	1.52	19.40	6.08	81.48	31.86	153.73	39.83	451.55	1.74	0.06	20.88	0.16	1.74	976.6
DHG-1-40	0.05	19.28	0.16	2.45	7.23	1.93	42.51	16.77	218.28	86.42	400.83	94.91	959.60	4.10	0.05	19.28	0.16	4.10	2476.3

5. Depositional Age of No. 6 Coal and Its Geological Implications

Generally, for the Phanerozoic strata, the youngest concordant U–Pb age of a detrital zircon can reveal the maximum age of sedimentary strata [8,9,25]. U–Pb isotopic data for zircon grains in the No. 6 coal from the Heidaigou coal mine yielded a weighted average age of 293.0 ± 1.5 Ma, which was younger than the biostratigraphic age of sandstone in the bottom of the Taiyuan Formation (302 Ma) [26] and the same as the paleopalynology data reported by Yang et al. [18] and Jia [27]. They found the early Permian T. multinervis and Gulisprites–Thymosporites in the No. 6 coal from the Heidaigou coalmine [18,27]. As the geochemistry discussed above, these magmatic zircons with their REE results were similar to zircons in the late Carboniferous–early Permian volcanic tuffs, which are widely distributed in North China, i.e., Western Liaoning [26], Eastern Hebei [27], Northern Shanxi [28], Daqingshan [29], and Western Beijing [30], and they had a main rock association of andesite, dacite, trachydacite, and rhyolite [27–31]. Cope et al. [32] analyzed a tuff sample from the Upper Carboniferous Taiyuan Formation in the Yangkeleng coal mine, which is northeast of the Heidaigou coal mine, and five well-zoned euhedral zircons yielded a U–Pb concordia age of 290 ± 6 Ma. Zhang et al. [30] conducted fourteen zircon grains' dating in tuff samples from the Upper Permian Hongmaoling Formation, Beijing Xishan, and the $^{206}Pb/^{238}U$ analysis showed a weighted mean age of 296 ± 4 Ma. These data are all in good agreement with those from the No. 6 coal in the Heidiagou coal mine, indicating that Late Paleozoic volcanoes once existed in the northern margin of North China [33,34]. In addition, some others have researched the detrital zircon grains in the sandstones of Taiyuan Formation, and many contemporaneous zircon grains have been discovered. In Beijing Xishan, east of the Heidaigou Mine, Yang et al. [35] reported the two youngest zircon grains with ages of 304 ± 4 Ma in the middle of the Taiyuan Formation. Li et al. [36] represented the two youngest detrital zircons with an average age of 304 ± 6 Ma for a sandstone sample in the upper Taiyuan Formation, Ningwu-Jingle Basin, southeast of the Heidaigou Mine. These two samples were located lower than the No. 6 coal seam. However, Sun et al. [37] reported abundant 302–293 Ma detrital zircon grains from Jinci sandstone and 301–277 Ma from Qiligou sandstone in the bottom and middle of the Taiyuan Formation in the Taiyuan Xishan Coalfield. These differences may be the results of the diachronism of the Taiyuan Formation. Compared with the International Chronostratigraphic Chart [38], the Carboniferous–Permian boundary in the Jungar Coalfield should be located below the No. 6 coal.

6. Conclusions

This study presented the U–Pb ages and rare earth element compositions of zircon grains from the No. 6 coal in the Heidaigou Mine, Jungar Coalfield. The CL images and Th/U ratios of zircon grains implied that they had the characteristics of magmatic zircon. These magmatic zircon grains with a single peak age yielded a $^{206}Pb/^{238}U$ weighted mean age of 293.0 ± 1.5 Ma (MSWD = 1.5), indicating that the depositional age of the No. 6 coal was 293.0 ± 1.5 Ma. The Carboniferous–Permian boundary should be located stratigraphically lower than the No. 6 coal. In addition, Heidaigou No. 6 coal has a high content of gallium, and an accurate age also can provide a good guide for the source of gallium in No. 6 coal.

Author Contributions: Conceptualization, methodology, validation, investigation, resources, data curation, C.L. and X.C.; writing-original draft preparation, C.L.; writing-review and editing, C.L., B.S. and F.Z.; visualization, supervision, project administration, funding acquisition, C.L. and B.S. All authors have read and agreed to the published version of the manuscript.

Funding: This research was funded by the National Natural Science Foundation of China (Grant Nos. 42172193, 2021YFC2902002, 41802184) and the Natural Science Foundation of Shanxi Province, China (Grant No. 201801D121031).

Institutional Review Board Statement: Not applicable.

Informed Consent Statement: Not applicable.

Data Availability Statement: The data presented in this study are available on request from the authors. The data are not publicly available due to original informed consent provisions.

Acknowledgments: We gratefully acknowledge two anonymous reviewers and the editor-in-chief for their extensive and constructive comments that helped to improve this manuscript significantly.

Conflicts of Interest: The authors declare no conflict of interest.

References

1. Tripathy, G.R.; Hannah, J.L.; Stein, H.J.; Geboy, N.J.; Ruppert, L.F. Radiometric dating of marine-influenced coal using Re–Os geochronology. *Earth Planet. Sci. Lett.* **2015**, *432*, 13–23. [CrossRef]
2. Gu, D.J.; Han, D.X. Study of coal-forming age and sedimentary rate by magnetic stratigraphic method. *J. China Univ. Min. Technol.* **1989**, *18*, 1–5.
3. Petersen, H. The petroleum generation potential and effective oil window of humic coals related to coal composition and age. *Int. J. Coal Geol.* **2006**, *67*, 221–248. [CrossRef]
4. Petersen, H.; Nytoft, H. Oil generation capacity of coals as a function of coal ages and aliphatic structure. *Org. Geochem.* **2006**, *37*, 558–583. [CrossRef]
5. Cirilli, S. Upper Triassic-lowermost Jurassic palynology and palynostratigraphy: A review. *Geol. Soc. Lond. Spec. Publ.* **2010**, *334*, 285–314. [CrossRef]
6. Fildani, A.; Weislogel, A.; Drinkwater, N.; McHargue, T.; Tankard, A.; Wooden, J.; Hodgson, D.; Flint, S. U-Pb zircon ages from the southwestern Karoo basin, South Africa-Implications for the Permian-Triassic boundary. *Geology* **2009**, *37*, 719–722. [CrossRef]
7. Rotich, E.K.; Handler, M.R.; Sykes, R.; Selby, D.; Naeher, S. Depositional influences on Re-Os systematics of Late Cretaceous–Eocene fluvio-deltaic coals and coaly mudstones, Taranaki Basin, New Zealand. *International J. Coal Geol.* **2021**, *236*, 103670. [CrossRef]
8. Andersen, T. Detrital zircons as tracers of sedimentary provenance: Limiting conditions from statistics and numerical simulation. *Chem. Geol.* **2005**, *216*, 249–270. [CrossRef]
9. Dickinson, W.R.; Gehrels, G.E. Use of U-Pb ages of detrital zircons to infer maximum depositional ages of strata: A test against a Colorado Plateau Mesozoic database. *Earth Planet. Sci. Lett.* **2009**, *288*, 115–125. [CrossRef]
10. Gehrels, G. Detrital Zircon U-Pb Geochronology Applied to Tectonics. *Annu. Rev. Earth Planet. Sci.* **2014**, *42*, 127–149. [CrossRef]
11. Wilson, A.H.; Zeh, A. U-Pb and Hf isotopes of detrital zircons from the Pongola Supergroup: Constraints on deposition ages, provenance and Archean evolution of the Kaapvaal craton. *Precambrian Res.* **2018**, *305*, 177–196. [CrossRef]
12. Barbeau, D.L.; Ducea, M.N.; Gehrels, G.E.; Kidder, S.; Wetmore, P.H.; Saleeby, J.B. U-Pb detrital-zircon geochronology of northern Salinian basement and cover rocks. *Geol. Soc. Am. Bull.* **2005**, *117*, 466–481. [CrossRef]
13. Jones, J.V.; Connelly, J.N.; Karlstrom, K.E.; Williams, M.L.; Doe, M.F. Age, provenance, and tectonic setting of Paleoproterozoic quartzite successions in the southwestern United States. *Geol. Soc. Am. Bull.* **2006**, *121*, 247–264. [CrossRef]
14. Dai, S.F.; Ren, D.Y.; Li, S.S. Discovery of the superlarge gallium ore deposit in Jungar, Inner Mongolia, North China. *Chin. Sci. Bull.* **2006**, *51*, 2243–2252. [CrossRef]
15. Dai, S.F.; Li, D.; Chou, C.L.; Zhao, L.; Zhang, Y.; Ren, D.Y.; Ma, Y.W.; Sun, Y.Y. Mineralogy and geochemistry of boehmite-rich coals: New insights from the Haerwusu Surface Mine, Jungar Coalfield, Inner Mongolia, China. *Int. J. Coal Geol.* **2008**, *74*, 185–202. [CrossRef]
16. Wang, W.F.; Qin, Y.; Liu, X.H.; Zhao, J.L.; Wang, J.Y.; Wu, G.D.; Liu, J.T. Distribution, occurrence and enrichment causes of gallium in coals from the Jungar Coalfield, Inner Mongolia. *Sci. China-Earth Sci.* **2011**, *54*, 1053–1068. [CrossRef]
17. Wang, S.J. Sporo-pollen assemblages from the Late Craboniferous and Early Permian coal series in Yaogou colliery, Zhungeer banner, Neimenggu Autonomous region. *J. China Coal Soc.* **1982**, *2*, 36–50, (In Chinese with English abstract).

18. Yang, G.X.; Chen, Z.H.; Zhang, S.L. The flora's characteristics of Taiyuan Formation and Shanxi Formation of the eastern Zhuangeerqi, Inner Mongol. *J. Earth Sci. China* **1983**, *4*, 69–83, (In Chinese with English abstract).
19. Jia, G.L. Dating and regional correlation of sporopollen of No.6 coal seam, Jungar coalfield, Inner Mongolia. *Coal Geol. China* **1994**, *6*, 21–24, (In Chinese with English abstract).
20. *GB/T 482-2008*; Sampling of Coal in Seam. National Standard of P.R. China: Beijing, China, 2008. (In Chinese)
21. Zhao, G.C.; Sun, M.; Wilde, S.A.; Li, S.Z. Late Archean to Paleoproterozoic evolution of the North China Craton: Key issues revisited. *Precambr. Res.* **2005**, *136*, 177–202. [CrossRef]
22. Liu, Y.S.; Hu, Z.C.; Gao, S.; Günther, D.; Xu, J.; Gao, C.G.; Chen, H.H. In situ, analysis of major and trace elements of anhydrous minerals by LA-ICP-MS without applying an internal standard. *Chem. Geol.* **2008**, *257*, 34–43. [CrossRef]
23. Ludwig, K.R. *Isoplot/Ex Version 4: A Geochronological Toolkit for Microsoft Excel*; Geochronology Center: Berkeley, CA, USA, 2011.
24. Belousova, E.; Griffin, W.; O'Reilly, S.Y.; Fisher, N. Igneous zircon: Trace element composition as an indicator of source rock type. *Contrib. Mineral. Petrol.* **2002**, *143*, 602–622. [CrossRef]
25. Zeh, A.; Gerdes, A. U–Pb and Hf isotope record of detrital zircons from gold-bearing sediments of the Pietersburg Greenstone Belt (South Africa)—Is there a common provenance with the Witwatersrand Basin? *Precambrian Res.* **2012**, *204*, 46–56. [CrossRef]
26. Li, B.F.; Wen, X.D.; Li, G.D. High resolution sequence stratigraphy analysis on the Permo-Carboniferous in north China platform. *Geosci. Front.* **1999**, *6*, 81–94, (In Chinese with English abstract).
27. Jia, B.W.; Guo, C.Y. Study on pyroclastic rocks of Late Paleozoic coal measures, Eastern Hebei, China. *Acta Sedimentol. Sin.* **1993**, *11*, 65–74, (In Chinese with English abstract).
28. Zhong, R.; Sun, S.P.; Chen, F.; Fu, Z.M. The discovery of rhyo-tuffite in the Taiyuan Formation and stratigraphic correlation of the Daqingshan and Datong coalfields. *Acta Geosci. Sin.* **1995**, *16*, 291–301, (In Chinese with English abstract).
29. Zhou, A.C.; Jia, B.W.; Ma, M.L.; Zhang, H. The whole sequences of volcanic event deposits on the north margin of the North China plate and their features. *Geol. Rev.* **2001**, *47*, 175–183, (In Chinese with English abstract).
30. Zhang, S.H.; Zhao, Y.; Song, B.; Yang, Y.H. Zircon SHRIMP U–Pb and in-situ Lu–Hf isotope analyses of a tuff from Western Beijing: Evidence for missing Late Paleozoic arc volcano eruptions at the northern margin of the North China block. *Gondwana Res.* **2007**, *12*, 157–165. [CrossRef]
31. Zhang, S.H.; Zhao, Y.; Liu, J.M.; Hu, Z.C. Different sources involved in generation of continental arc volcanism: The Carboniferous–Permian volcanic rocks in the northern margin of the North China block. *Lithos* **2016**, *240*, 382–401. [CrossRef]
32. Cope, T.; Ritts, B.; Darby, B.; Fildani, B.; Graham, S.A. Late Paleozoic Sedimentation on the Northern Margin of the North China Block: Implications for Regional Tectonics and Climate Change. *Int. Geol. Rev.* **2005**, *47*, 270–296. [CrossRef]
33. Zhang, S.H.; Zhao, Y.; Liu, X.C.; Liu, D.Y.; Chen, F.K.; Xie, L.W.; Chen, H.H. Late Paleozoic to Early Mesozoic mafic-ultramafic complexes from the northern North China Block: Constraints on the composition and evolution of the lithospheric mantle. *Lithos* **2009**, *110*, 229–246. [CrossRef]
34. Ma, S.X.; Meng, Q.R.; Duan, L.; Wu, G. Reconstructing Late Paleozoic exhumation history of the Inner Mongolia Highland along the northern edge of the North China Craton. *J. Asian Earth Sci.* **2014**, *87*, 89–101. [CrossRef]
35. Yang, J.H.; Wu, F.Y.; Shao, J.A.; Wilde, S.A.; Xie, L.W.; Liu, X.M. Constraints on the timing of uplift of the Yanshan Fold and Thrust Belt, North China. *Earth Planet. Sci. Lett.* **2006**, *246*, 336–352. [CrossRef]
36. Li, H.Y.; Xu, Y.G.; Huang, X.L.; Zhen, Y. Activation of northern margin of the North China Craton in Late Paleozoic: Evidence from U-Pb dating and Hf isotopes of detrital zircons from the Upper Carboniferous Taiyuan Formation in the Ningwu-Jingle basin. *Chin. Sci. Bull.* **2009**, *54*, 677–686. [CrossRef]
37. Sun, B.L.; Zeng, F.G.; Liu, C.; Cui, X.Q.; Wang, W. Constraints on U-Pb dating of detrital zircon of the maximum depositional age for Upper Paleozoic coal-bearing strata in Xishan, Taiyuan and its stratigraphic significance. *Acta Geol. Sin.* **2014**, *88*, 185–197, (In Chinese with English abstract).
38. Cohen, K.F.; Finney, S.C.; Gibbard, P.L.; Fan, J.X. The ICS International Chronostratigraphic Chart. *Episodes* **2018**, *36*, 199–204. [CrossRef]